Site-Isolated Pt-SBA15 Materials from Tris(*tert*-butoxy)siloxy Complexes of Pt(II) and Pt(IV)

Daniel A. Ruddy,[†,‡] Jonggol Jarupatrakorn,[¶,†,‡] Robert M. Rioux,[§] Jeffrey T. Miller,[⊥] Meredith J. McMurdo,[†,‡] Jennifer L. McBee,[†,‡] Karl A. Tupper,[†] and T. Don Tilley*[,†,‡]

Department of Chemistry, University of California, Berkeley, Berkeley, California 94720, Chemical Sciences Division, Lawrence Berkeley National Laboratory, 1 Cyclotron Road, Berkeley, California 94720, Department of Chemical Engineering, Pennsylvania State University, University Park, Pennsylvania 16802, BP Research Center, E-1F, 150 West Warrenville Road, Naperville, Illinois 60565, Advanced Photon Source, Argonne National Laboratory, 9700 South Cass Avenue, Argonne, Illinois 60439

Received June 12, 2008. Revised Manuscript Received July 18, 2008

Two novel tris(*tert*-butoxy)siloxy complexes of Pt(II) and Pt(IV) were prepared in high yields, (cod)Pt[OSi(O^{t}Bu)$_3$]$_2$ (**1**; 87%; cod = 1,5-cyclooctadiene) and Me$_3$Pt(tmeda)[OSi(O^{t}Bu)$_3$] (**2**; 81%; tmeda = *N*,*N*,*N*′,*N*′-tetramethylethylenediamine). The structures of these compounds were determined by multinuclear NMR spectroscopy and by single-crystal X-ray analysis. The thermolytic chemistry of **1** and **2** in the solid state was studied by thermogravimetric analysis. The thermal decomposition of these complexes resulted in the formation of Pt metal, with the elimination of HOSi(O^{t}Bu)$_3$. Precursors **1** and **2** react with the surface Si−OH groups of mesoporous SBA15 silica to generate surface-supported Pt centers. The coordination environments of the supported Pt centers in these new materials, termed Pt(II)SBA15 and Pt(IV)SBA15, were investigated using Fourier-transform infrared spectroscopy, X-ray absorption near-edge spectroscopy, and extended X-ray absorption fine structure analysis. These materials were also characterized using N_2 porosimetry, powder X-ray diffraction and transmission electron microscopy. Comparisons with the molecular precursors **1** and **2** revealed many similarities, and the results are indicative of isolated Pt(II) and Pt(IV) centers. In addition, isolated Pt centers proved to be robust in inert atmosphere to 150−200 °C, which is similar to the decomposition temperatures of **1** and **2**.

Introduction

The stabilization and characterization of isolated catalytic sites has played a major role in the strategic design of new catalysts that exhibit improved performance.[1−3] Numerous investigations have focused on site-isolated early transition metal centers on an oxide support, and key factors governing catalytic function have been determined (e.g., active site structure, catalytic mechanism, catalytic intermediates). Notable examples include reports from Basset,[4,5] Marks,[6−8] Corma,[9] and others[10−14] on the introduction of metal centers onto an oxide surface via mild conditions. These materials have been used as catalysts for a variety of reactions, including oxidation, polymerization, hydrogenation, dehydrogenation, and alkene/alkane metathesis.

Catalysis with oxide-supported late transition metal nanoparticles has been extensively studied,[15−19] but much less research has focused on the isolation of mononuclear late transition metal centers.[20] The latter type of supported site is of interest with respect to comparisons of stability and reactivity with related metallic nanoparticles and bulk metal. For example, recent reports attribute catalytic activity in the water−gas-shift reaction ($CO + H_2O \rightarrow CO_2 + H_2$) to the presence of supported cationic Au and Pt active sites, rather than metallic Au or Pt.[21,22] In addition, it has been demonstrated that a single atom of Pd on MgO facilitates the cyclotrimerization of acetylene.[23] Gates has provided

* Corresponding author. E-mail: tdtilley@berkeley.edu.
† University of California, Berkeley.
‡ Lawrence Berkeley National Laboratory.
§ Pennsylvania State University.
|| BP Research Center.
⊥ Argonne National Laboratory.
¶ Current address: Department of Chemistry, Mahidol University, Bangkok 10400, Thailand.

(1) Thomas, J. M.; Raja, R.; Lewis, D. W. *Angew. Chem., Int. Ed.* **2005**, *44*, 6456.
(2) Corma, A. *Chem. Rev.* **1997**, *97*, 2373.
(3) Volta, J. C. *Top. Catal.* **2001**, *15*, 121.
(4) Basset, J. M.; Choplin, A. *J. Mol. Catal.* **1983**, *21*, 95.
(5) Coperet, C.; Chabanas, M.; Saint-Arroman, R. P.; Basset, J. M. *Angew. Chem., Int. Ed.* **2003**, *42*, 156.
(6) Ahn, H.; Marks, T. J. *J. Am. Chem. Soc.* **2002**, *124*, 7103.
(7) Ahn, H.; Nicholas, C. P.; Marks, T. J. *Organometallics* **2002**, *21*, 1788.
(8) Nicholas, C. P.; Marks, T. J. *Langmuir* **2004**, *20*, 9456.
(9) Corma, A.; Navarro, M. T.; Pariente, J. P. *Chem. Commun.* **1994**, 147.
(10) Thomas, J. M. *Top. Catal.* **2001**, *15*, 85.
(11) Maschmeyer, T.; Rey, F.; Sankar, G.; Thomas, J. M. *Nature* **1995**, *378*, 159.
(12) Sinclair, P. E.; Sankar, G.; Catlow, C. R. A.; Thomas, J. M.; Maschmeyer, T. *J. Phys. Chem. B* **1997**, *101*, 4232.
(13) Moses, A. W.; Raab, C.; Nelson, R. C.; Leifeste, H. D.; Ramsahye, N. A.; Chattopadhyay, S.; Eckert, J.; Chmelka, B. F.; Scott, S. L. *J. Am. Chem. Soc.* **2007**, *129*, 8912.
(14) Nenu, C. N.; van Lingen, J. N. J.; de Groot, F. M. F.; Koningsberger, D. C.; Weckhuysen, B. M. *Chem.−Eur. J.* **2006**, *12*, 4756.
(15) Haller, G. L. *J. Catal.* **2003**, *216*, 12.
(16) Ono, Y. *Catal. Today* **2003**, *81*, 3.
(17) Hayek, K.; Fuchs, M.; Klotzer, B.; Reichl, W.; Rupprechter, G. *Top. Catal.* **2000**, *13*, 55.
(18) Efstathiou, A. M.; Verykios, X. E. *Appl. Catal., A* **1997**, *151*, 109.
(19) Lowenthal, E. E.; Allard, L. F.; Te, M.; Foley, H. C. *J. Mol. Catal. A* **1995**, *100*, 129.

10.1021/cm801598k CCC: $40.75
Published on Web 09/24/2008

important contributions in this area utilizing X-ray absorption spectroscopy to investigate the structure and catalytic properties of small Ir, Pt, and Au clusters and of mononuclear Pt and Au centers on oxide supports.[24−29]

Supported mononuclear Pt centers are particularly interesting due to the diversity of chemical transformations associated with Pt catalysts, including hydrocarbon/alcohol oxidations,[30,31] hydrocarbon isomerizations,[32,33] alkane hydrogenolysis,[34,35] and selective alkene/arene hydrogenations.[35,36] However, the formation of Pt metal nanoparticles on an oxide support is a relatively facile process. This is evident by numerous reports describing the synthesis of Pt−MO_x materials via the introduction of a simple Pt salt (i.e., K_2PtCl_4, K_2PtCl_6, $Pt(NH_3)_4(NO_3)_2$), followed by a calcination procedure that results in crystallization of Pt nanoparticles.[37−42] In contrast, state-of-the-art synthetic processes, such as mass-selected cluster deposition under ultrahigh vacuum conditions, have been utilized to support small, well-defined Pt clusters or a mononuclear Pt center.[43,44] This advanced technique requires complex instrumentation, and therefore, solution-based synthetic routes to introduce uniform, mononuclear Pt centers would facilitate further studies of this interesting system.

Research from this laboratory has demonstrated that the thermolytic molecular precursor (TMP) method is an effective approach for introduction of various transition metal centers (e.g., Ti(IV), Fe(III), V(V), Ta(V)) on an oxide support under nonaqueous conditions.[45−47] In addition, these precursors serve as excellent structural and spectroscopic models for the supported centers derived therefrom. With respect to late transition metals, Co(II), Rh(III), and Cu(I) complexes that incorporate the tris(*tert*-butoxy)siloxy ligand, −$OSi(O^tBu)_3$, have been investigated as precursors to catalytic materials.[48−50] For example, the molecular precursor $[CuOSi(O^tBu)_3]_4$ was used to introduce catalytically active Cu(I) centers on silica, and it was demonstrated that the Cu species retain the +1 oxidation state after grafting.[49,51,52]

This report describes the synthesis and characterization of two platinum tris(*tert*-butoxy)siloxy complexes, $(cod)Pt[OSi(O^tBu)_3]_2$ (**1**) and $Me_3Pt(tmeda)[OSi(O^tBu)_3]$ (**2**). These complexes were utilized as the Pt source to introduce isolated Pt(II) and Pt(IV) centers on the surface of mesoporous silica, SBA15. In addition, they act as molecular models for Pt(II) and Pt(IV) sites, respectively. The structures of the supported Pt centers were compared to those of **1** and **2** using Fourier transform infrared (FTIR) spectroscopy, X-ray absorption near-edge spectroscopy (XANES), and extended X-ray absorption fine structure (EXAFS) analysis. The thermal stability of the supported Pt centers was investigated, and the catalytic activity of the PtSBA15 materials in olefin hydrogenation was studied.

Experimental Section

General Procedures. All manipulations were conducted under a nitrogen atmosphere using standard Schlenk techniques or in a Vacuum Atmospheres drybox unless otherwise noted. Dry, oxygen-free solvents were used throughout. Dichloro(1,5-cyclooctadiene-)platinum(II) and iodotrimethylplatinum(IV) were purchased from Strem Chemicals, Inc. and used as received. Styrene and cyclohexene were purchased from Aldrich and dried over CaH_2 prior to use. Hydrogen (99.999%) was purchased from Praxair. The following were prepared according to literature procedures: $Me_3Pt(tmeda)(OSO_2CF_3)$,[53] $HOSi(O^tBu)_3$,[54] $NaOSi(O^tBu)_3$,[55] $KOSi(O^tBu)_3$,[56] and SBA15.[57]

(20) Notable examples include (a) Ermakov, Y. I.; Kuznetsov, B. N.; Ryndin, Y. A.; Lazutkin, A. M. *Kinet. Katal.* **1973**, *14*, 709. (b) Ermaov, Y. I.; Kuznetsov, B. N.; Karakchiev, L. G.; Derbeneva, S. S. *Kinet. Katal.* **1973**, *14*, 1594. (c) Ermakov, Y. I.; Kuznetsov, B. N. *React. Kinet. Catal. Lett.* **1974**, *1*, 87. (d) Ryndin, Y. A.; Kuznetsov, V. L.; Kuznetsov, B. N.; Ermakov, Y. I. *Nefti Neftekhim.* **1974**, 113. (e) Kuznetsov, B. N.; Ermakov, Y. I.; Kuznetsov, V. L.; Ryndin, Y. A.; Karakchiev, L. G.; Shinkarenko, V. G.; Mamaeva, E. K.; Startseva, L. Y. *Kinet. Katal.* **1975**, *16*, 1356. (f) Richmond, M. K.; Scott, S. L.; Alper, H. *J. Am. Chem. Soc.* **2001**, *123*, 10521. (g) Berthoud, R.; Baudouin, A.; Fenet, B.; Lukens, W.; Pelzer, K.; Basset, J.-M.; Candy, J.-P.; Coperet, C. *Chem.−Eur. J.* **2008**, *14*, 3523.

(21) Fu, Q.; Saltsburg, H.; Flytzani-Stephanopoulos, M. *Science* **2003**, *301*, 935.

(22) Fu, Q.; Deng, W. L.; Saltsburg, H.; Flytzani-Stephanopoulos, M. *Appl. Catal., B* **2005**, *56*, 57.

(23) Abbet, S.; Sanchez, A.; Heiz, U.; Schneider, W. D.; Ferrari, A. M.; Pacchioni, G.; Rosch, N. *J. Am. Chem. Soc.* **2000**, *122*, 3453.

(24) Alexeev, O.; Gates, B. C. *Top. Catal.* **2000**, *10*, 273.

(25) Guzman, J.; Gates, B. C. *Angew. Chem., Int. Ed.* **2003**, *42*, 690.

(26) Argo, A. M.; Odzak, J. F.; Gates, B. C. *J. Am. Chem. Soc.* **2003**, *125*, 7107.

(27) Enderle, B. A.; Labouriau, A.; Ott, K. C.; Gates, B. C. *Nano Lett.* **2002**, *2*, 1269.

(28) Guzman, J.; Gates, B. C. *Nano Lett.* **2001**, *1*, 689.

(29) Guzman, J.; Gates, B. C. *Langmuir* **2003**, *19*, 3897.

(30) Yamada, Y. M. A.; Arakawa, T.; Hocke, H.; Uozumi, Y. *Angew. Chem., Int. Ed.* **2007**, *46*, 704.

(31) Wang, W.; Stagg-Williams, S. M.; Noronha, F. B.; Mattos, L. V.; Passos, F. B. *Catal. Today* **2004**, *98*, 553.

(32) Hayek, K.; Goller, H.; Penner, S.; Rupprechter, G.; Zimmermann, C. *Catal. Lett.* **2004**, *92*, 1.

(33) Nieminen, V.; Karhu, H.; Kumar, N.; Heinmaa, I.; Ek, P.; Samoson, A.; Salmi, T.; Murzin, D. Y. *Phys. Chem. Chem. Phys.* **2004**, *6*, 4062.

(34) Cho, I. H.; Park, S. B.; Cho, S. J.; Ryoo, R. *J. Catal.* **1998**, *173*, 295.

(35) Rioux, R. M.; Song, H.; Hoefelmeyer, J. D.; Yang, P.; Somorjai, G. A. *J. Phys. Chem. B* **2005**, *109*, 2192.

(36) Kirm, I.; Medina, F.; Sueiras, J. E.; Salagre, P.; Cesteros, Y. *J. Mol. Catal. A* **2007**, *261*, 98.

(37) Matsuhashi, H.; Nishiyama, S.; Miura, H.; Eguchi, K.; Hasegawa, K.; Iizuka, Y.; Igarashi, A.; Katada, N.; Kobayashi, J.; Kubota, T.; Mori, T.; Nakai, K.; Okazaki, N.; Sugioka, M.; Umeki, T.; Yazawa, Y.; Lu, D. L. *Appl. Catal., A* **2004**, *272*, 329.

(38) Radivojevic, D.; Seshan, K.; Lefferts, L. *Appl. Catal., A* **2006**, *301*, 51.

(39) Iida, H.; Kondo, K.; Igarashi, A. *Catal. Commun.* **2006**, *7*, 240.

(40) Eswaramoorthy, M.; Niwa, S.; Toba, M.; Shimada, H.; Raj, A.; Mizukami, F. *Catal. Lett.* **2001**, *71*, 55.

(41) Lopez, T.; Bosch, P.; Moran, M.; Gomez, R. *J. Phys. Chem.* **1993**, *97*, 1671.

(42) Zhang, G. D.; Coq, B.; Demenorval, L. C.; Tichit, D. *Appl. Catal., A* **1996**, *147*, 395.

(43) Heiz, U.; Sherwood, R.; Cox, D. M.; Kaldor, A.; Yates, J. T. *J. Phys. Chem.* **1995**, *99*, 8730.

(44) Heiz, U.; Sanchez, A.; Abbet, S.; Schneider, W. D. *J. Am. Chem. Soc.* **1999**, *121*, 3214.

(45) Fujdala, K. L.; Brutchey, R. L.; Tilley, T. D. In *Topics in Organometallic Chemistry*; Coperet, C., Chaudret, B., Eds.; Springer-Verlag: New York, 2005; vol. *16*, p 69−116.

(46) Ruddy, D. A.; Ohler, N. L.; Bell, A. T.; Tilley, T. D. *J. Catal.* **2006**, *238*, 277.

(47) Brutchey, R. L.; Lugmair, C. G.; Schebaum, L. O.; Tilley, T. D. *J. Catal.* **2005**, *229*, 72.

(48) Jarupatrakorn, J.; Tilley, T. D. *Dalton Trans.* **2004**, 2808.

(49) Fujdala, K. L.; Drake, I. J.; Bell, A. T.; Tilley, T. D. *J. Am. Chem. Soc.* **2004**, *126*, 10864.

(50) Brutchey, R. L.; Drake, I. J.; Bell, A. T.; Tilley, T. D. *Chem. Commun.* **2005**, 3736.

(51) Drake, I. J.; Fujdala, K. L.; Bell, A. T.; Tilley, T. D. *J. Catal.* **2005**, *230*, 14.

(52) Drake, I. J.; Fujdala, K. L.; Baxamusa, S.; Bell, A. T.; Tilley, T. D. *J. Phys. Chem. B* **2004**, *108*, 18421.

(53) Gschwind, R. M.; Schlecht, S. *Dalton Trans.* **1999**, 1891.

(54) Abe, Y.; Kijima, I. *Bull. Chem. Soc. Jpn.* **1969**, *42*, 1118.

(55) McMullen, A. K.; Tilley, T. D.; Rheingold, A. L.; Geib, S. J. *Inorg. Chem.* **1989**, *28*, 3772.

Characterization. Benzene-d_6 was purified and dried by vacuum distillation from sodium/potassium alloy. Solution ^{1}H, ^{13}C, and ^{195}Pt NMR spectra were recorded at 400, 100, and 86 MHz, respectively, using a Bruker AVB-400 spectrometer. Chemical shifts for ^{1}H and ^{13}C NMR spectra were referenced internally to the residual solvent signal relative to tetramethylsilane. ^{195}Pt NMR spectra were referenced to a Na_2PtCl_6 standard in D_2O. Nitrogen adsorption isotherms were obtained using a Quantachrome Autosorb 1, and samples were outgassed at 120 °C for at least 15 h prior to measurement. The Brunauer−Emmet−Teller (BET) method[58] was used to determine surface areas, and the Barrett−Joyner−Halenda method[59] was used to obtain pore size distributions. Thermal analyses were performed on a TA Instruments SDT 2960 Integrated TGA/DSC (differential scanning calorimetry) analyzer with a heating rate of 10 °C min^{-1} under a flow of nitrogen or oxygen. Calcinations were performed using a Lindberg 1200 °C three-zone furnace with a heating rate of 10 °C min^{-1} under a flow of nitrogen. Carbon and hydrogen elemental analyses were performed by the College of Chemistry microanalytical laboratory at the University of California, Berkeley. Platinum elemental analyses were performed at Galbraith Laboratories, Inc. (Knoxville, TN) by means of inductively coupled plasma optical emission spectroscopy (ICP-OES). Powder X-ray diffraction (PXRD) experiments were performed on a Siemens D5000 X-ray diffractometer using Cu Kα radiation. Small-angle X-ray scattering (SAXS) data were collected using a Bruker Nanostar spectrometer using Cu Kα radiation. Transmission electron microscopy (TEM) was carried out on a Philips Tecnai 12 transmission electron microscope operating at 200 kV. Samples for TEM studies were prepared by depositing a hexane suspension of the material onto a carbon-coated copper grid obtained from Ted Pella, Inc. The mesoporous support, SBA15, was characterized by PXRD and N_2 porosimetry prior to catalyst preparation (surface area, 575 m^2 g^{-1}; pore volume, 1.19 cc g^{-1}; average pore radius, 6.0 nm). The hydroxyl group concentration of the SBA15 was determined to be 2.1(1) OH nm^{-2}, via reaction of SBA15 with $Mg(CH_2C_6H_5)_2\cdot 2THF$ and quantification of the evolved toluene by ^{1}H NMR spectroscopy.

The single-crystal X-ray analyses of compounds **1** and **2** were carried out at the UC Berkeley CHEXRAY crystallographic facility. All measurements were made on a Bruker SMART or APEX CCD area detector with graphite-monochromated Mo Kα radiation (λ = 0.710 69 Å). The frame data were integrated by the program SAINT (SAX Area-Detector Integration Program; V4.024; Siemens Industrial Automation, Inc.: Madison, WI, 1995) and corrected for Lorentz and polarization effects. Data were analyzed for agreement and possible absorption using XPREP. Empirical absorption corrections based on comparison of redundant and equivalent reflections were applied using SADABS. The structures were solved using the SHELXTL crystallographic software package of Molecular Structure Corporation using direct methods or Patterson methods and expanded with Fourier techniques. Unless stated otherwise, all non-hydrogen atoms were refined anisotropically, and the hydrogen atoms were placed in calculated positions but not refined. Disorder was observed in the *tert*-butoxy groups of both **1** and **2**. The function minimized in the full-matrix least-squares refinement was $\Sigma w(F_0 - F_c)$. The weighting scheme was based on counting statistics and included a *p*-factor to downweight the intense reflections.

Infrared spectra were recorded on a Nicolet Nexus 6700 FTIR spectrometer with a liquid-nitrogen-cooled MCT-B detector. Measurements were made at 4.0 cm^{-1} resolution. The sample cell was similar to that previously reported.[60,61] CaF_2 windows (25 mm diameter × 15 mm thickness) were obtained from ISP Optics (Irvington, NY). Samples (20−25 mg) were pressed at 1000 psi for 10 s to produce 25 mm diameter self-supporting wafers. Prior to analysis, samples were dehydrated under a flow of He (50 mL min^{-1}) at 75 °C for 30 min and cooled to 25 °C.

X-ray absorption measurements were made on the insertion-device beam line of the Materials Research Collaborative Access Team (MRCAT) at the Advanced Photon Source, Argonne National Laboratory. A cryogenically cooled double-crystal Si (111) monochromator was used in conjunction with an uncoated glass mirror to minimize the presence of harmonics. The monochromator was scanned continuously during the measurements with data points integrated over 0.5 eV for 0.05 s per data point. Measurements were made in transmission mode at the Pt L_{III} absorption edge (11.564 keV) with the ionization chambers optimized for the maximum current with linear response (~10^{10} photons detected per second) using a mixture of N_2 and He in the incident X-ray detector and a mixture of ~20% Ar in N_2 in the transmission X-ray detector. A Pt foil spectrum was acquired simultaneously with each measurement for energy calibration. Phase shift and backscattering amplitudes were obtained from reference compounds ($Na_2Pt(OH)_6$ for Pt−O and Pt foil for Pt−Pt). Standard procedures based on WINXAS97 software were used to extract the EXAFS data. The coordination parameters were obtained by a least-squares fit in *k*- and *R*-space of the isolated multiple-shell, k^2-weighted Fourier transform data.

Catalyst samples were handled in the absence of air using a glovebag purged with Ar and were pressed into a cylindrical holder of ~5 mm diameter with a thickness chosen to give a total absorbance (μx) of ~ 2.0, corresponding to ~20 mg of catalyst, which resulted in a Pt edge step ($\Delta\mu x$) of ~0.5 for 2 wt % Pt on SBA15. The sample holder was loaded in a quartz tube (1 in. diameter) and fitted with Swagelok fittings containing Kapton windows for entry and exit of X-rays. X-ray absorption spectra of fresh samples were obtained in flowing He (50 mL min^{-1}), and heat treatments were conducted from room temperature to 250 °C. These samples were heated in He for a predetermined amount of time and then cooled to room temperature in He before measurement of the X-ray absorption spectra. Initial fits of the supported Pt centers on SBA15 were based on the bond distances and coordination numbers from the X-ray crystal structures. The known coordination numbers were fixed, and the Debye−Waller factor (DWF) was determined. These DWF values were fixed and used in the remaining analyses. Small changes in structure due to heat treatment were determined by the difference file technique (e.g., subtraction of the modified spectrum from the original spectrum). The difference file reflects only the changes in structure that occur during heat treatment. Peaks that are larger in the spectra for the modified materials have normal amplitude functions, but are 180° out of phase with the reference. Peaks that are smaller in the subtracted spectra have normal phase and amplitude functions.

(56) Terry, K. W.; Su, K.; Tilley, T. D.; Rheingold, A. L. *Polyhedron* **1998**, *17*, 891.
(57) Zhang, H.; Sun, J. M.; Ma, D.; Bao, X. H.; Klein-Hoffmann, A.; Weinberg, G.; Su, D. S.; Schlogl, R. *J. Am. Chem. Soc.* **2004**, *126*, 7440.
(58) Brunauer, S.; Emmett, P. H.; Teller, E. *J. Am. Chem. Soc.* **1938**, *60*, 309.
(59) Barrett, E. P.; Joyner, L. G.; Halenda, P. P. *J. Am. Chem. Soc.* **1951**, *73*, 373.
(60) Drake, I. J.; Zhang, Y. H.; Gilles, M. K.; Liu, C. N. T.; Nachimuthu, P.; Perera, R. C. C.; Wakita, H.; Bell, A. T. *J. Phys. Chem. B* **2006**, *110*, 11665.
(61) Joly, J. F.; Zanierszydlowski, N.; Colin, S.; Raatz, F.; Saussey, J.; Lavalley, J. C. *Catal. Today* **1991**, *9*, 31.

(cod)Pt[OSi(O^{t}Bu)$_3$]$_2$ (1). A benzene solution (20 mL) of KOSi(O^{t}Bu)$_3$ (0.328 g, 1.08 mmol) was added to a benzene solution (20 mL) of (cod)PtCl$_2$ (0.203 g, 0.543 mmol) at room temperature. After 16 h at room temperature, the solvent was removed in vacuo. The product was extracted from the KCl with pentane (3 × 20 mL). Concentration (10 mL) and cooling at −30 °C afforded **1** as an opaque colorless solid (0.391 g, 87%). Recrystalliztion at −35 °C by vapor diffusion of acetonitrile into a toluene solution of **1** resulted in crystals suitable for X-ray structure analysis. Anal. Calcd for $C_{32}H_{66}O_8PtSi_2$: C, 46.3; H, 8.01. Found: C, 46.4; H, 8.17. ^{1}H NMR (400 MHz, benzene-d_6, 20 °C) δ 5.69 (br, 4H, =C*H*), 1.85 (m, 4H, exo CH_2), 1.57 (s, 54H, OCMe_3), 1.27 (m, 4H, endo CH_2). ^{13}C{^{1}H} NMR (100 MHz, benzene-d_6, 20 °C) δ 89.6, 71.7, 32.2, 30.1. ^{29}Si NMR (99.35 MHz, benzene-d_6, 20 °C): −88.17 (s, O*Si*(O^{t}Bu)$_3$).^{195}Pt{^{1}H} NMR (86 MHz, benzene-d_6, 20 °C) δ −2857. IR (KBr, cm^{-1}) 2974 s, 2929 s, 1474 m, 1434 m, 1387 m, 1363 m, 1244 m, 1197 m, 1043 vs, 1020 vs, 825 m, 705 s, 654 w. mp 150−151 °C (dec).

Me$_3$Pt(tmeda)[OSi(O^{t}Bu)$_3$] (2). A toluene solution (20 mL) of NaOSi(O^{t}Bu)$_3$ (0.142 g, 0.50 mmol) was added to a toluene solution (20 mL) of Me$_3$Pt(tmeda)(OTf) (0.250 g, 0.50 mmol) at 0 °C. The reaction was stirred at 0 °C for 15 min and then allowed to reach room temperature with stirring over 18 h. The precipitate was removed by filtration and washed with pentane (2 × 10 mL). The solvent was removed in vacuo, yielding a colorless solid. Recrystallization of the product from a concentrated pentane solution (10 mL) at −78 °C yielded **2** as colorless, block-shaped crystals (0.250 g, 81%). Anal. Calcd for $C_{21}H_{52}N_2O_4PtSi$: C, 40.69; H, 8.46; N, 4.52. Found: C, 40.70; H, 8.54; N, 4.51. ^{1}H NMR (400 MHz, benzene-d_6, 20 °C) δ 2.55 (t, 6H, $^3J_{Pt-H}$ = 8.4 Hz, NMe_2), 2.28 (m, 2H, CH_2N), 1.75 (t, 6H, $^3J_{Pt-H}$ = 14.8 Hz, NMe_2), 1.61 (m, 2H, CH_2N), 1.59 (s, 27H, OCMe_3), 1.35 (t, 6H, $^2J_{Pt-H}$ = 72.0 Hz, PtMe_2), 0.41 (t, 3H, $^2J_{Pt-H}$ = 71.2 Hz, Pt*Me*). ^{13}C{^{1}H} NMR (100 MHz, benzene-d_6, 20 °C) δ 70.6, 60.3, 48.0, 46.2, 32.4, −6.6 (t, $^1J_{Pt-C}$ = 713.8 Hz, PtMe_2), −11.8 (t, $^1J_{Pt-C}$ = 781.4 Hz, Pt*Me*).^{29}Si NMR (99.35 MHz, benzene-d_6, 20 °C): −93.51 (s, O*Si*(O^{t}Bu)$_3$).^{195}Pt{^{1}H} NMR (86 MHz, benzene-d_6, 20 °C) δ −1999. IR (KBr, cm^{-1}) 2967 vs, 2897 vs, 1473 m, 1458 m, 1383 w, 1358 m, 1236 m, 1197 s, 1050 vs, 1021 vs, 817 w, 800 w, 689 w. mp 176−179 °C (dec).

Preparation of Pt(II)SBA15. The SBA15 was dried at 120 °C in vacuo for 12 h and handled under a nitrogen atmosphere. A 250 mg sample of SBA15 was suspended in pentane (20 mL), and a pentane solution (20 mL) of **1** (21.3 mg, 0.0256 mmol) was added at room temperature. The mixture was stirred for 16 h and then filtered and washed with pentane (3 × 20 mL). The colorless material was dried in vacuo for 2 h prior to storage in a drybox. The wt % Pt loading was determined to be 1.83 wt % by ICP methods.

Preparation of Pt(IV)SBA15. The SBA15 was dried at 120 °C in vacuo for 12 h and handled under a nitrogen atmosphere. A 250 mg sample of SBA15 was suspended in pentane (20 mL), and a pentane solution (20 mL) of **2** (15.9 mg, 0.0257 mmol) was added at room temperature. The mixture was stirred for 16 h and then filtered and washed with pentane (3 × 20 mL). The colorless material was dried in vacuo for 2 h prior to storage in a drybox. The wt % Pt loading was determined to be 1.93 wt % by ICP methods.

Catalytic Hydrogenation of Styrene with PtSBA15. A sample of PtSBA15 catalyst (~0.010 g) was added to a J. Young NMR tube in a drybox. Benzene-d_6 (0.50 mL) and styrene (12 μL, 0.10 mmol) were added via syringe. Ferrocene (0.010 g) was added as an internal standard. After three freeze−pump−thaw cycles, hydrogen (1 atm, ~0.10 mmol) was added at room temperature. The reaction was heated in an oil bath at 50 °C for 24 h. Substrate conversion and product assignment were determined via ^{1}H NMR spectroscopy.

Catalytic Hydrogenation of Cyclohexene with PtSBA15. A sample of PtSBA15 catalyst (~0.010 g) was added to a J. Young NMR tube in a drybox. Benzene-d_6 (0.50 mL) and cyclohexene (10 μL, 0.099 mmol) were added via syringe. Ferrocene (0.010 g) was added as an internal standard. After three freeze−pump−thaw cycles, hydrogen (1 atm, ~0.10 mmol) was added at room temperature. The reaction was heated in an oil bath at 50 °C. Substrate conversion and product assignment were determined via ^{1}H NMR spectroscopy.

Catalytic Hydrogenation with 1. Complex **1** (0.0050 g, 0.0060 mmol) was added to a J. Young NMR tube and dissolved in benzene-d_6 (0.50 mL). Styrene (69 μL, 0.60 mmol, 100 equiv vs **1**) or cyclohexene (61 μL, 0.60 mmol, 100 equiv vs **1**) was added via syringe. Ferrocene (0.010 mg) was added as an internal standard. After three freeze−pump−thaw cycles, hydrogen (1 atm, ~0.10 mmol) was added at room temperature. The reaction was heated in an oil bath at 50 °C. Substrate conversion and product assignment were determined via ^{1}H NMR spectroscopy.

Catalytic Hydrogenation with 2. Complex **2** (0.0050 g, 0.0080 mmol) was added to a J. Young NMR tube and dissolved in benzene-d_6 (0.50 mL). Styrene (92 μL, 0.80 mmol, 100 equiv vs **2**) or cyclohexene (81 μL, 0.80 mmol, 100 equiv vs **2**) was added via syringe. Ferrocene (0.010 mg) was added as an internal standard. After three freeze−pump−thaw cycles, hydrogen (1 atm, ~0.10 mmol) was added at room temperature. The reaction was heated in an oil bath at 50 °C. Substrate conversion and product assignment were determined via ^{1}H NMR spectroscopy.

Results and Discussion

Synthesis and Characterization of 1 and 2. The reaction of (cod)PtCl$_2$ with 2 equiv of KOSi(O^{t}Bu)$_3$ in benzene afforded the tris(*tert*-butoxy)siloxy platinum(II) complex, (cod)Pt[OSi(O^{t}Bu)$_3$]$_2$ (**1**; eq 1), isolated in 87% yield as an opaque colorless solid from cold (−30 °C) pentane.

$$\text{(cod)PtCl}_2 + 2\text{KOSi(O}^t\text{Bu)}_3 \xrightarrow{C_6H_6} \text{(cod)Pt[OSi(O}^t\text{Bu)}_3\text{]}_2\text{(1)} + 2\text{KCl} \quad (1)$$

The room temperature ^{1}H NMR spectrum of **1** in benzene-d_6 exhibits a singlet due to the *tert*-butoxy protons at 1.58 ppm, indicative of equivalent −OSi(O^{t}Bu)$_3$ ligands. The vinylic protons of the cod ligand resonate at 5.70 ppm with ^{195}Pt satellites (J_{PtH} = 65 Hz). The ^{13}C{^{1}H}, ^{29}Si, and ^{195}Pt NMR spectra are consistent with the ^{1}H NMR spectrum. These multinuclear NMR spectroscopic data support the proposed structure of a *cis* square planar geometry, according to the usual chelating behavior of the cod ligand.

The reaction of Me$_3$Pt(tmeda)(OTf) with 1 equiv of NaOSi(O^{t}Bu)$_3$ in toluene afforded the tris(*tert*-butoxy)siloxy platinum(IV) complex, Me$_3$Pt(tmeda)[OSi(O^{t}Bu)$_3$] (**2**; eq 2), isolated in 81% yield from cold (−78 °C) pentane as colorless crystals.

$$\text{Me}_3\text{Pt(tmeda)(OTf)} + \text{NaOSi(O}^t\text{Bu)}_3 \xrightarrow{\text{toluene}} \text{Me}_3\text{Pt(tmeda)[OSi(O}^t\text{Bu)}_3\text{]}\text{(2)} + \text{NaOTf} \quad (2)$$

The room temperature ^{1}H NMR spectrum of **2** in benzene-d_6 exhibits one resonance at 1.59 ppm corresponding to the −OSi(O^{t}Bu)$_3$ group. The three platinum-bound methyl

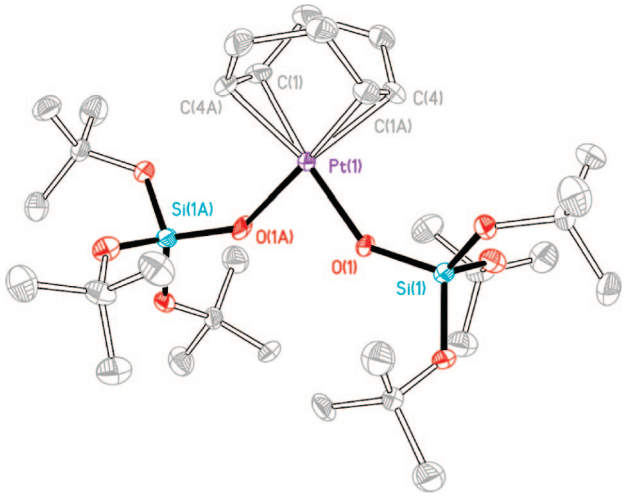

Figure 1. Molecular structure of **1** with thermal ellipsoids at 50% probability. One of the two independent molecules is shown with hydrogen atoms removed for clarity.

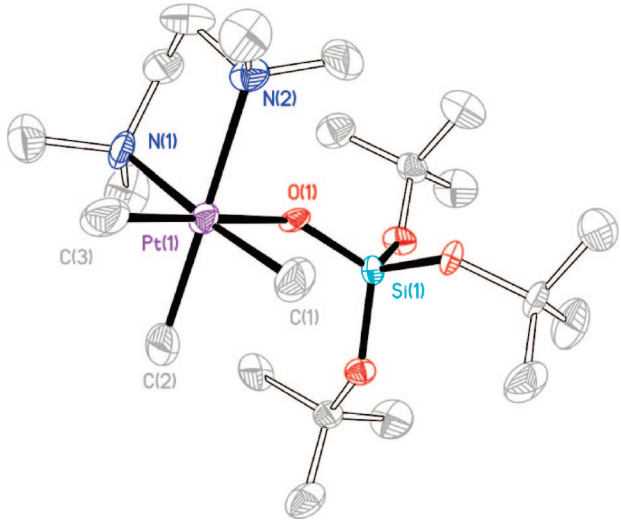

Figure 2. Molecular structure of **2** with thermal ellipsoids at 50% probability. Hydrogen atoms are removed for clarity.

groups are believed to be facially coordinated as in $Me_3Pt(tmeda)(OTf)$.[53] Two Pt−CH_3 resonances are observed at 1.35 and 0.41 ppm (J_{PtH} = 72.0 and 71.2 Hz, respectively). The 2:1 ratio of protons allows for their assignment as two equivalent methyl groups *trans* to the tmeda ligand and a single methyl group *trans* to the siloxy ligand, respectively. The tmeda methyl resonances also exhibit ^{195}Pt satellites and are observed at 2.55 and 1.75 ppm, and the ethylene resonances were observed at 2.28 and 1.61 ppm. The $^{13}C\{^1H\}$, ^{29}Si, and ^{195}Pt NMR spectra are consistent with the ^{1}H NMR spectrum.

The molecular structures of **1** and **2** were unequivocally determined by single-crystal X-ray analysis. The structure of **1** confirms the *cis* square planar geometry at Pt, which is consistent with the NMR spectroscopic analysis (Figure 1). The structure of **2** confirms the facial arrangement of the platinum-bound methyl groups on an octahedrally coordinated Pt center (Figure 2). Selected bond distances and angles are presented in Table 1, and crystallographic data is presented in Table S1 of the Supporting Information. In general, the Pt−C and Pt−N bond distances and angles in

Table 1. Selected Bond Distances (Å) and Angles (°) for 1 and 2

distances		angles	
(cod)Pt[OSi(O^{t}Bu)$_3$]$_2$ (**1**)			
Pt(1)−O(1)	1.982(7)	O(1)−Pt(1)−C(1A)	96.2(3)
Pt(1)−C(1)	2.12(1)	O(1)−Pt(1)−C(4)	93.1(3)
Pt(1)−C(4)	2.137(6)	O(1A)−Pt(1)−O(1)	83.6(4)
C(1)−C(4A)	1.33(1)	Si(1)−O(1)−Pt(1)	144.0(4)
O(1)−Si(1)	1.592(7)		
Me$_3$Pt(tmeda)[OSi(O^{t}Bu)$_3$] (**2**)			
Pt(1)−O(1)	2.140(7)	C(1)−Pt(1)−C(2)	85.4(6)
Pt(1)−C(1)	2.01(1)	C(1)−Pt(1)−C(3)	88.3(5)
Pt(1)−C(2)	2.04(1)	C(3)−Pt(1)−C(2)	87.0(5)
Pt(1)−C(3)	2.04(1)	C(1)−Pt(1)−O(1)	92.6(4)
Pt(1)−N(1)	2.217(9)	N(1)−Pt(1)−N(2)	82.2(3)
Pt(1)−N(2)	2.247(9)	C(1)−Pt(1)−N(2)	94.7(4)
O(1)−Si(1)	1.560(7)	C(3)−Pt(1)−N(1)	95.2(5)
		Si(1)−O(1)−Pt(1)	138.8(4)

complexes **1** and **2** are similar to those of the few reported structures of Pt(II) and Pt(IV) complexes with silsesquioxane or triaryl- or trialkylsiloxy ligands.[62−64] In particular, the structure of **1** is very similar to that of a (cod)Pt(II)-silsesquioxane derivative, and these complexes display similar Pt−O and Pt−C bond distances.[65] Typical Pt−OSi bond distances range from 1.93 to 2.05 Å. The Pt−OSi bond distance in **1** is within this range: 1.982(7) Å. Interestingly, the Pt−OSi bond distance in **2** was found to be slightly longer at 2.140(7) Å. A similar Pt−OSi bond distance of 2.129(3) Å was observed for a *trans*-bis(triethylphosphine)phenyl(silsesquioxane) platinum(II) complex with a monodentate silsesquioxane ligand.[66] The elongated Pt−OSi bond was attributed to the strong *trans* influence of the phenyl ligand and the electron-withdrawing effect of the silsesquioxane group. In **2**, the siloxy ligand is *trans* to a methyl group, whereas in the previously reported Pt(II) complexes, the siloxy ligand is *trans* to a cod ligand or another siloxy ligand. The strong *trans* influence of the methyl group may induce a lengthening of the Pt-OSi bond distance; however, steric reasons must also be considered due the bulk of the tris(*tert*-butoxy)siloxy ligand.

Solid-State Thermolytic Chemistry of 1 and 2. The thermal decomposition behavior of compounds **1** and **2** was examined by thermogravimetric analysis (TGA) under an inert atmosphere (N_2). The TGA traces for **1** and **2** are given in Figure 3. For compound **1**, the onset of decomposition occurs at ∼160 °C and is followed by a precipitous weight loss. The ceramic yield at 500 °C for the decomposition of **1** is 22.7%, which is considerably lower than that expected for Pt·2SiO_2 (38.0%) or Pt·SiO_2 (30.7%). However, the observed ceramic yield is similar to that expected for Pt metal (23.5%). This result is likely due to loss of HOSi(O^{t}Bu)$_3$ as a volatile elimination product. To test for this, the volatile elimination products formed from the decomposition of solid **1** under vacuum at 275 °C for 2 h were condensed into an

(62) Abbenhuis, H. C. L.; Burrows, A. D.; Kooijman, H.; Lutz, M.; Palmer, M. T.; Van Santen, R. A.; Spek, A. L. *Chem. Commun.* **1998**, 2627.
(63) Kim, K. M.; Sohn, Y. S. *Inorg. Chem.* **1998**, *37*, 6109.
(64) Fukuoka, A.; Sato, A.; Kodama, K.; Hirano, M.; Komiya, S. *Inorg. Chim. Acta* **1999**, *294*, 266.
(65) Quadrelli, E. A.; Davies, J. E.; Johnson, B. F. G.; Feeder, N. *Chem. Commun.* **2000**, 1031.
(66) Mintcheva, N.; Tanabe, M.; Osakada, K. *Organometallics* **2006**, *25*, 3776.

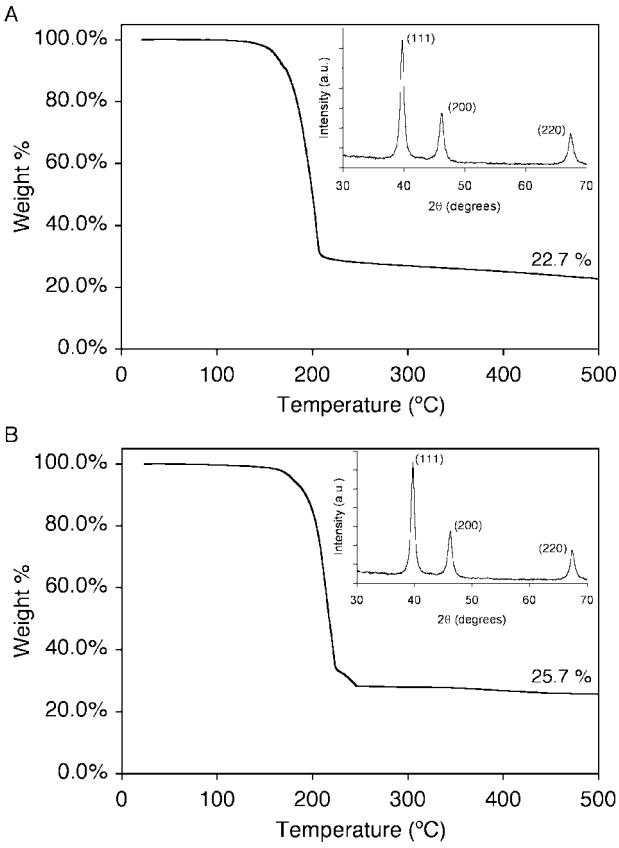

Figure 3. TGA traces for (A) **1** and (B) **2** under N_2 with a heating rate of 10 °C min^{-1}. The insets are the PXRD patterns for the decomposition products (fcc Pt).

NMR tube containing benzene-d_6 and a ferrocene standard at −196 °C, and 1.8 equiv of $HOSi(O^tBu)_3$ was observed. For compound **2**, the onset of decomposition occurs at ∼180 °C, again followed by a precipitous weight loss. The ceramic yield at 500 °C for the decomposition of **2** is 25.7%, which is well below the expected ceramic yield for $Pt{\cdot}SiO_2$ (41.2%) and is also lower than the expected ceramic yield for the formation of Pt metal (31.5%). Interestingly, when the volatile elimination products from the decomposition of **2** under vacuum at 275 °C for 2 h were collected, 50% of the added amount of precursor complex sublimed into the NMR tube (which was cooled at −196 °C). The volatility of **2** accounts for the reduced ceramic yield for this compound. The loss of $HOSi(O^tBu)_3$ as an elimination product also contributes to a ceramic yield that is less than expected for $Pt{\cdot}SiO_2$. This is supported by analysis of the decomposition products from **2** at 275 °C for 2 h in a sealed vial under a nitrogen atmosphere. After cooling to room temperature, the elimination products were extracted with benzene-d_6 and transferred into an NMR tube containing a ferrocene standard, and 0.9 equiv of $HOSi(O^tBu)_3$ was observed. The analyses of the elimination products provide strong evidence that the loss of $HOSi(O^tBu)_3$ results in ceramic yields that are lower than expected for Pt/Si/O materials. Furthermore, powder X-ray diffraction analyses of the black solid decomposition products from **1** and **2** displayed characteristic peaks for crystalline fcc Pt^0 (Figure 3, inset), supporting the assignment of the formation of Pt metal upon decomposition of the precursors.

DSC was also used to monitor the decomposition of **1** and **2** under nitrogen. For both precursors, an endothermic transition associated with the beginning of decomposition is observed, and the transitions are centered at 171 °C for **1** and at 182 °C for **2** (Figure S1 of the Supporting Information). Following the endothermic transition, an exothermic transition is observed for both precursors. The exotherms are centered at 245 °C and are associated with a gradual weight loss. Decomposition under an oxygen atmosphere does not alter the onset temperature or ceramic yield for either complex. However, the endothermic transition is not observed for decomposition under oxygen. Rather, the decomposition is accompanied by an exothermic reaction, presumably the Pt-catalyzed combustion of organic byproducts, which results in an abnormal shape of the TGA traces over the range of temperatures where decomposition occurs (Figure S2 of the Supporting Information).

The thermolysis behavior of **1** and **2** is clearly different from that of the previously studied group IV metal siloxides, $M[OSi(O^tBu)_3]_4$ (M = Ti, Zr, Hf), which display an abrupt weight loss with the formation of isobutene (12 equiv), water (6 equiv), and the theoretical ceramic yield for $MO_2{\cdot}4SiO_2$ materials.[45] These decompositions are catalyzed by Brønsted and Lewis acids and proceed via alkene elimination. This process presumably produces M−O−Si−OH species that then undergo condensations (via elimination of H_2O) to form the multicomponent oxide material.[45] The decompositions of **1** and **2**, however, result in elimination of $HOSi(O^tBu)_3$ and formation of Pt metal. This suggests a different mechanism of decomposition which may involve Pt−O bond homolysis, as suggested for thermolysis of the late metal siloxide complex $[CuOSi(O^tBu)_3]_4$.[49,67] Similarly, silanol and Rh metal were observed in the thermolysis of $\{(cod)Rh[OSi(O^tBu)_3]\}_2$.[48] Thus, the thermolytic chemistry of late transition-metal (alkoxy)siloxy complexes seems to differ substantially from that of analogous early transition-metal complexes.

Synthesis of Pt(II)SBA15 and Pt(IV)SBA15. The mesoporous silica SBA15 was prepared according to a literature procedure.[57] Precursors **1** and **2** were grafted onto the silica surface by adding a pentane solution of the precursor to a stirred pentane suspension of SBA15 under nitrogen at room temperature. Low concentrations of **1** and **2** (2.5−2.6 mM per gram of SBA15) were employed to ensure low weight percent platinum−silica materials (∼2.0 wt %) with a high spatial dispersity of Pt centers on the surface (∼0.10 Pt nm^{-2}).[47,68,69] After 16 h, the solid was filtered, washed with pentane, and dried in vacuo at room temperature to yield the colorless materials Pt(II)SBA15 and Pt(IV)SBA15. The weight percent of Pt was determined to be 1.83 and 1.93 wt %, respectively, by ICP-OES.

Solution ^1H NMR spectroscopy was used to monitor the reactions of **1** and **2** with SBA15. The reaction of surface Si−OH groups with a solution of excess **1** or **2** should result in the elimination of $HOSi(O^tBu)_3$ via protonolysis at the

(67) Terry, K. W.; Lugmair, C. G.; Gantzel, P. K.; Tilley, T. D. *Chem. Mater.* **1996**, *8*, 274.
(68) Jarupatrakorn, J.; Tilley, J. D. *J. Am. Chem. Soc.* **2002**, *124*, 8380.
(69) Nozaki, C.; Lugmair, C. G.; Bell, A. T.; Tilley, T. D. *J. Am. Chem. Soc.* **2002**, *124*, 13194.

Scheme 1. Surface Grafting Chemistry of 1 and 2 with SBA15

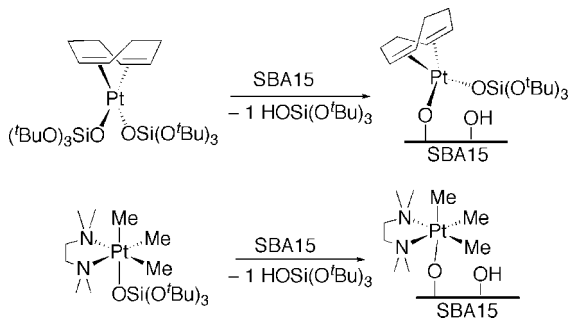

Table 2. Platinum Loading and Nitrogen Porosimetry Data for PtSBA15 Materials

material	Pt content (wt % Pt)	Pt coverage (Pt nm^{-2})	S_{BET} (m^2 g^{-1})	r_{pore} (nm)	V_{pore} (cc g^{-1})
SBA15			575	6.0	1.19
Pt(II)SBA15	1.83	0.098	395	5.7	1.00
Pt(IV)SBA15	1.93	0.104	415	5.7	1.01

Pt−OSi bond. Compound **2** offers the additional possibility of the elimination of CH_4 via protonolysis at the Pt−CH_3 bond. The observed elimination product of the reaction between **1** and SBA15 in benzene-d_6 at room temperature was identified as HOSi(O^{t}Bu)$_3$. This reaction generated 1.0 equiv of silanol per equivalent of reacted **1** (versus a ferrocene internal standard) (Scheme 1). On the basis of the amount of **1** consumed, the maximum loading of Pt was determined to be 15.3 wt % (0.82 Pt nm^{-2}). For compound **2**, the sole elimination product observed upon reaction with SBA15 in benzene-d_6 was also HOSi(O^{t}Bu)$_3$. There was no evidence for the elimination of methane. Similar to the reaction of **1** with SBA15, 1.0 equiv of silanol was eliminated on the basis of **2** consumed in the grafting reaction, and the maximum loading of Pt was determined to be 16.7 wt % (0.88 Pt nm^{-2}) (Scheme 1).

Characterization of Pt(II)SBA15 and Pt(IV)SBA15. Nitrogen porosimetry was used to evaluate the surface areas and pore structure of the new materials. The adsorption−desorption data for each material correspond to type IV isotherms, which are characteristic of mesoporous SBA15 materials.[57,70] The surface area, pore volume, and pore radius data for the materials are presented in Table 2. The pore size distribution was relatively narrow, and the average pore radii were determined from the adsorption isotherm. As expected, the Pt-containing materials have surface areas that are reduced relative to that of SBA15, but the pore radii are similar. In addition, the mesostructured architecture was confirmed by observation of the small-angle (100) reflection in the powder X-ray scattering pattern and when viewed by transmission electron microscopy (TEM, Figure S3 of the Supporting Information).

The surface structures for these silica-supported platinum materials appear to be similar to the molecular structures of the precursor complexes; thus, **1** and **2** represent good models of mononuclear Pt centers supported on silica. FTIR spectroscopy can be used to compare the structures of the surface-supported species with the molecular precursors. The FTIR spectrum of **1** contains peaks that are characteristic for C=C stretches of a Pt-bound cod ligand at 1474 and 1434 cm^{-1}. The positions of these peaks are similar to those reported for (cod)PtCl$_2$ (1479, 1432 cm^{-1}) and shifted from free cod (1487, 1426 cm^{-1}).[71] Analogous peaks at 1475 and 1435 cm^{-1} were observed in the FTIR spectrum of Pt(II)SBA15, which suggests that the supported Pt(II) coordination geometry is similar to that of **1** (Figure S4, Table S2 of the Supporting Information). The FTIR spectrum of **2** contains peaks that are distinctive for methyl C−H stretches (2967, 2897 cm^{-1}) and methyl C−H deformations (1473, 1458 cm^{-1}) of the Pt-CH_3 and N-CH_3 groups. Similarly, the FTIR spectrum of Pt(IV)SBA15 displays methyl C−H stretching peaks at 2964 and 2902 cm^{-1} and methyl C−H deformation peaks at 1475 and 1461 cm^{-1}. The observation of these peaks provides evidence that the Me_3Pt(tmeda) core is intact for the surface Pt(IV) species and that the supported Pt(IV) geometry is similar to that observed in **2** (Figure S4, Table S2 of the Supporting Information).

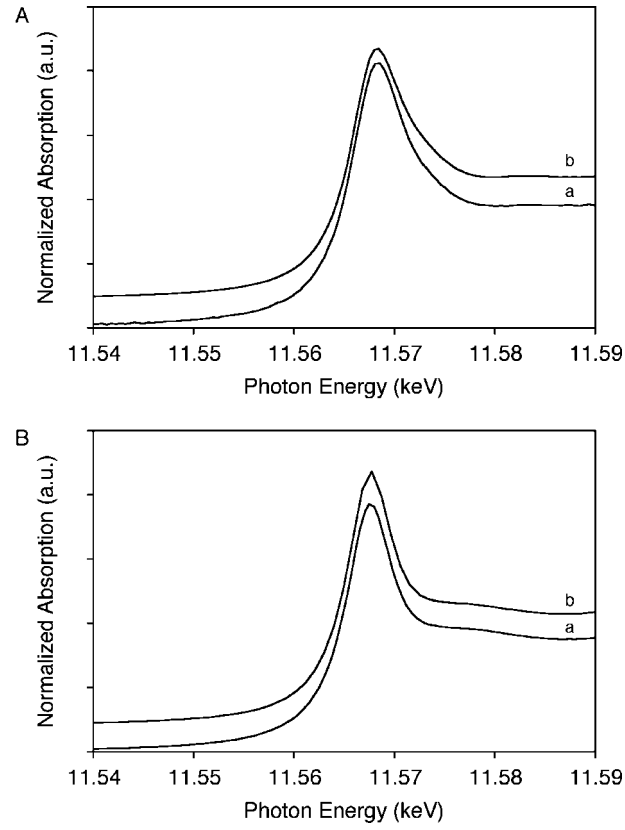

Figure 4. Pt L_{III} edge XANES spectra from 11.54 to 11.59 keV of (A) (a) **1** and (b) Pt(II)SBA15 and (B) (a) **2** and (b) Pt(IV)SBA15. The spectra are offset for clarity.

X-ray absorption spectroscopy provides additional evidence for the structural similarities between the precursors and the supported Pt centers. The Pt L_{III} edge XANES spectrum for Pt(II)SBA15 is identical to that for **1**, supporting the assignment of a surface-bound (cod)Pt(II) species (Figure 4A). Similarly, the Pt L_{III} edge XANES spectra for Pt(IV)SBA15 and **2** are identical, supporting the assignment

(70) Zhao, D. Y.; Huo, Q. S.; Feng, J. L.; Chmelka, B. F.; Stucky, G. D. *J. Am. Chem. Soc.* **1998**, *120*, 6024.

(71) Mink, J.; Keresztury, G. *Appl. Spectrosc.* **1993**, *47*, 1446.

Table 3. EXAFS Fitting Results for 1, 2, Pt(II)SBA15, and Pt(IV)SBA15

sample	shell[a]	N	R (Å)	σ^2 (Å^2)[b] ($\times 10^3$)	E_0 (eV)
1[c]	Pt−E	6	2.04	3.0	−0.4
Pt(II)SBA15[c]	Pt−E	6	2.06	3.0	−0.4
2[d]	Pt−E_{short}	3	2.01	3.0	−0.9
	Pt−E_{long}	3	2.28	3.0	3.5
Pt(IV)SBA15[d]	Pt−E_{short}	3	2.03	3.0	−0.8
	Pt−E_{long}	3	2.28	3.0	2.7

[a] C, N, and O are indistinguishable and are represented by E. [b] Debye−Waller factor. [c] k^2: Δk = 2.9−10.5 Å^{-1}, ΔR = 1.2−2.1 Å. [d] k^2: Δk = 2.9−10.4 Å^{-1}, ΔR = 1.2−2.3 Å.

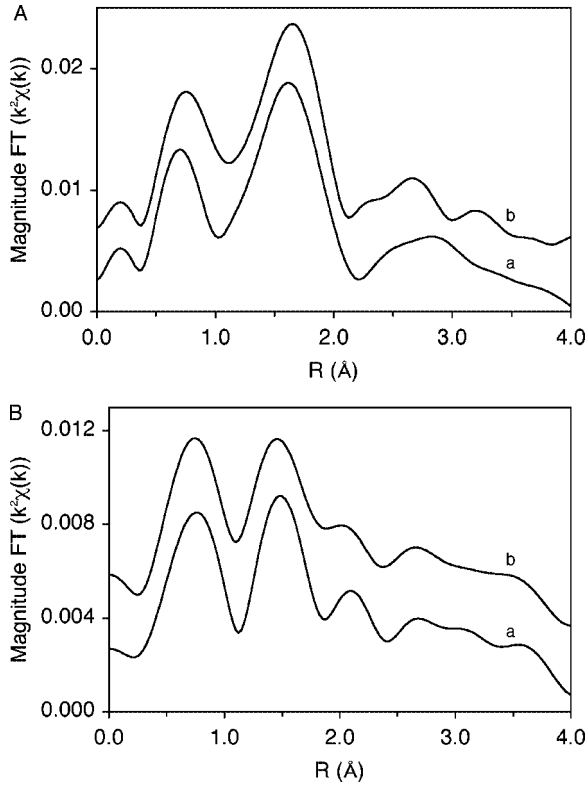

Figure 5. Magnitude of the Fourier transform for the k^2-weighted EXAFS function for (A) (a) **1** and (b) Pt(II)SBA15 (k:^{2} Δk = 2.5 − 10.5 Å^{-1}) and (B) (a) **2** and (b) Pt(IV)SBA15 at room temperature in He (k:^{2} Δk = 2.9 − 10.4 Å^{-1}). The spectra are offset for clarity.

of a surface-bound Me_3Pt(tmeda) species (Figure 4B). Since the phase shift and backscattering amplitudes are similar, assignments of C, N, and O atoms bound to Pt at similar bond distances cannot be determined using EXAFS. The EXAFS Pt-E (E = C, N, or O) coordination numbers and bond distances for the precursors and materials are consistent with those found in the X-ray crystal structures of **1** and **2**, respectively (Table 3). For example, the EXAFS spectra of **1** and Pt(II)SBA15 are identical with respect to first-shell scattering amplitude and position (Figure 5A). A Pt coordination number of 6 was determined with Pt−E bond distances of 2.04 Å for **1** and 2.06 Å for Pt(II)SBA15. This corresponds closely to the average of the four Pt−C and two Pt−O bond distances (2.08 Å) determined from the crystal structure of **1**. Similarly, EXAFS spectra of **2** and Pt(IV)SBA15 are very similar (Figure 5B). Fitting of the first shell gives a Pt coordination number of 6 with E atoms at two distances. The Pt(IV) coordination environment was modeled with three

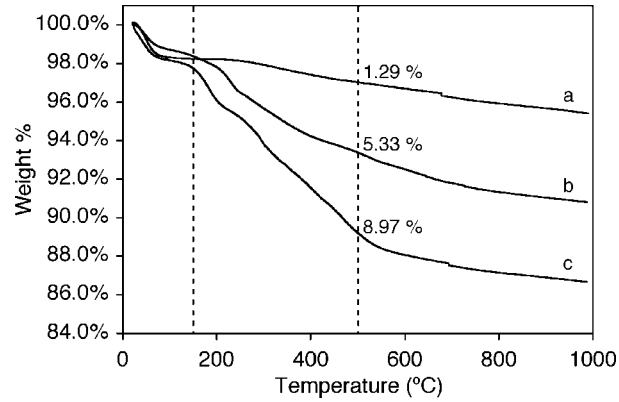

Figure 6. TGA traces for (a) SBA15, (b) Pt(IV)SBA15, and (c) Pt(II)SBA15 under N_2 with a heating rate of 10 °C min^{-1}. Dashed lines represent 150 and 500 °C, and the label denotes the observed weight percent loss in that temperature range.

short Pt−E bonds (2.01 Å for **2**, 2.03 Å for Pt(IV)SBA15) and three long Pt−E bonds (2.28 Å for both **2** and Pt(IV)SBA15) (Table 3). On the basis of the similarities of the bond distances determined by EXAFS to those in the crystal structure of **2**, the Pt−E_{short} bonds likely correspond to the three Pt−Me groups (2.01−2.04 Å), and the Pt−E_{long} bonds likely correspond to the Pt−N and Pt−O bonds (2.140−2.247 Å).

Thermolytic Chemistry of Supported Pt Centers. The stability of the silica-supported Pt centers toward decomposition was initially investigated by TGA. The TGA traces for SBA15, Pt(II)SBA15, and Pt(IV)SBA15 are depicted in Figure 6. A weight loss of 1.81% was observed for unmodified SBA15 below 150 °C, and the platinum−silica materials exhibited similar weight losses in this temperature region. This is associated with water that physisorbed to the silica surface upon transfer of the sample from the dry box to the instrument and does not represent decomposition of the Pt center.[72,73] The TGA traces for the platinum−silica materials under nitrogen exhibited features similar to those of the precursors **1** and **2**. The Pt(II)SBA15 material exhibited a moderate weight loss between 150 and 500 °C (8.97%; 7.68% after subtraction of the weight loss associated with unmodified SBA15). On the basis of the similarity of onset temperatures for Pt(II)SBA15 and **1**, this weight loss is assigned to decomposition of the supported (cod)Pt(II)[OSi(O^{t}Bu)$_3$] species. The observed weight loss was similar to the expected loss based on the Pt loading of 1.83 wt % and decomposition to form Pt metal. However, this more gradual weight loss suggests a less rapid decomposition for the supported Pt(II) center versus the rapid formation of platinum and HOSi(O^{t}Bu)$_3$ exhibited by the molecular precursor in the solid state. Similarly, the Pt(IV)SBA15 material exhibited a moderate weight loss between 150 and 500 °C (5.33%; 4.04% after subtraction of the weight loss associated with unmodified SBA15), and this corresponds closely to the expected weight loss for a Pt loading of 1.93 wt %. This weight loss is attributed to decomposi-

(72) Brutchey, R. L.; Ruddy, D. A.; Andersen, L. K.; Tilley, T. D. *Langmuir* **2005**, *21*, 9576.
(73) Ruddy, D. A.; Tilley, T. D. *Chem. Commun.* **2007**, 3350.

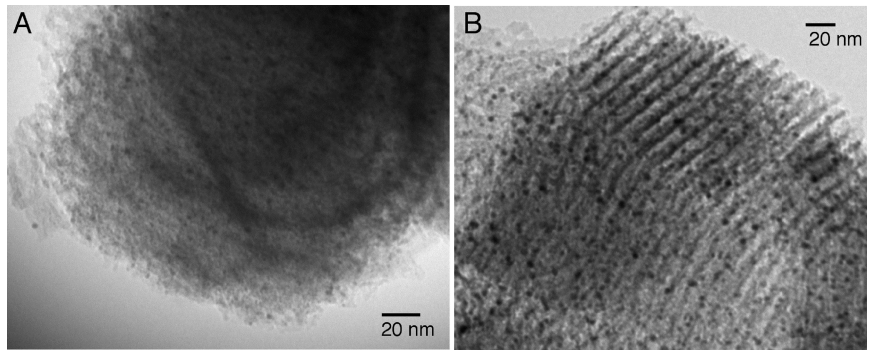

Figure 7. Representative TEM images of (A) Pt(II)SBA15$_{500}$ and (B) Pt(IV)SBA15$_{500}$.

tion of the $Me_3Pt(IV)(tmeda)$ species. Again, the weight loss occurred at an onset temperature similar to that observed for **2**, but the weight change was not as dramatic. Further weight loss of ~2.5% from 500 to 1000 °C was observed, which is similar to the weight loss that was observed for SBA15 (1.6%) over the same temperature range. This is attributed to dehydroxylation of the silica substrate (which was precalcined at 500 °C).

The thermal stability of the Pt centers was also probed using FTIR spectroscopy with in situ inert gas flow and temperature control. The intensities of the characteristic peaks for each material were followed as a function of temperature up to 200 °C under a flow of He (50 mL min^{-1}). A minimal decrease in peak intensity was observed under an inert atmosphere (He) while heating at 100 °C for 30 min. Further heat treatment of the samples at 150 and 200 °C for 30 min resulted in a more pronounced decrease in the peak intensities. Thus, the FTIR spectra are consistent with the TGA data and indicate that the supported Pt centers are robust to temperatures near the decomposition temperatures of the precursors and decompose slowly above 150 °C.

The formation of Pt metal after complete decomposition of the supported centers was confirmed by PXRD and TEM. Calcination of a sample of Pt(II)SBA15 under nitrogen at 500 °C for 2 h yielded the material Pt(II)SBA15$_{500}$. A color change from white to gray occurred during the heat treatment. The PXRD pattern of this material displayed broad, low-intensity diffraction peaks that are characteristic for crystalline fcc Pt^0. The broadness of the peaks suggests a small crystalline domain size near 3 nm, the detection limit of the instrument. Imaging by TEM revealed nanoparticles with an average diameter of 2.9(8) nm (Figure 7A). Similarly, calcination of a sample of Pt(IV)SBA15 under nitrogen at 500 °C for 2 h resulted in a gray material, termed Pt(IV)SBA15$_{500}$. The PXRD pattern of this material also displayed broad, low-intensity diffraction peaks indicative of small crystalline domains of Pt metal. TEM imaging revealed slightly larger Pt nanoparticles, with an average diameter of 4.0(9) nm (Figure 7B). These data suggest that the decomposition chemistry of the supported Pt centers resembles that of the precursors: thermolysis results in the formation of Pt metal.

It is possible that at lower decomposition temperatures (~250 °C), the supported centers may form small clusters and small nanoparticles. However, to identify clusters and particles smaller than 2−3 nm, PXRD and TEM are not the most effective techniques. PXRD is limited by peak broadening for small particles and small crystalline domains and will not detect noncrystalline Pt clusters. In addition, the thick, amorphous walls of SBA15 hinder resolution of small particles by TEM (≤2 nm diameter). X-ray absorption spectroscopy, on the other hand, offers excellent sensitivity for the identification of Pt−Pt interactions for noncrystalline species and for environments ranging from small clusters to nanoparticles (or larger).[74,75] In addition, this technique can be combined with in situ heat treatment to monitor changes in the coordination environment of the supported Pt centers after heat treatment and to detect the formation of Pt−Pt interactions at low calcination temperatures.

The Pt L_{III} edge XANES spectra for Pt(II)SBA15 and Pt(IV)SBA15 are presented in Figure 8 with the spectra for these materials after heat treatment in flowing He at 200 and 250 °C. The XANES spectra after 1 h heat treatments at 75, 100, and 150 °C were identical to the room temperature spectrum for each material, respectively. Up to 150 °C, fits of the EXAFS were also identical. A small decrease in absorption intensity was observed after heat treatment of Pt(II)SBA15 at 200 °C for 1 h, indicative of a change in the supported Pt environment (Figure 8A, trace b). This onset temperature for decomposition coincides with that observed by TGA. Further heat treatment at 250 °C for 1 h resulted in a more significant decrease in intensity, suggesting further decomposition of the supported Pt(II) site (Figure 8A, trace c). Similarly, a decrease in absorption intensity was observed for the Pt(IV)SBA15 material after heat treatment at 200 °C for 1 h, indicative of the beginning of decomposition. A more significant decrease in XANES intensity was observed after heat treatment at 250 °C for 1 h (Figure 8B, traces b and c).

EXAFS analysis confirms the structural changes for the supported Pt(IV) center after heat treatment. Fits of the EXAFS indicate partial reduction to metallic Pt (N_{Pt-Pt} = 2.5; R = 2.71 Å and N_{Pt-E} = 2.0 at 2.05 Å, Figure 9). Because the Pt is not fully reduced at 250 °C, the coordination number obtained in the fit does not represent the true N_{Pt-Pt} value from which the size of the metallic particles can be estimated. Several methods can be used to estimate the metallic coordination number. First, the XANES spectra can be fit with metallic Pt and an oxidized Pt reference. The choice for the oxidized Pt reference, however, is uncertain.

(74) Ramallo-Lopez, J. M.; Santori, G. F.; Giovanetti, L.; Casella, M. L.; Ferretti, O. A.; Requejo, F. G. *J. Phys. Chem. B* **2003**, *107*, 11441.
(75) Bazin, D. *Top. Catal.* **2002**, *18*, 79.

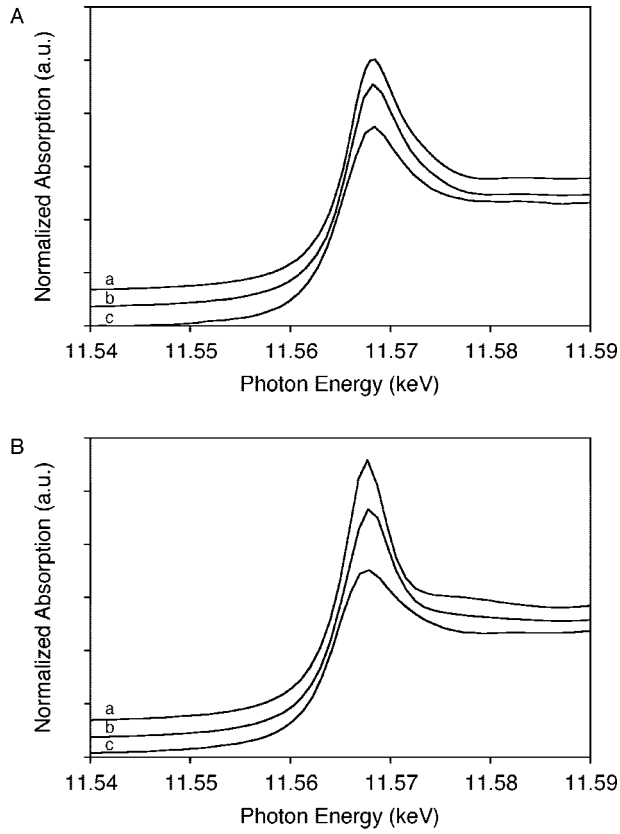

Figure 8. Pt L_{III} XANES spectra from 11.54 to 11.59 keV of (A) Pt(II)SBA15 in He at (a) room temperature (as-synthesized), (b) 200 °C, and (c) 250 °C; and (B) Pt(IV)SBA15 at (a) room temperature (as-synthesized), (b) 200 °C, and (c) 250 °C. The spectra are offset for clarity.

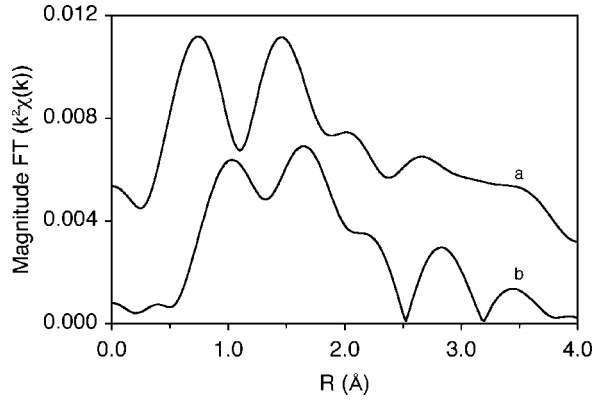

Figure 9. Magnitude of the Fourier transform for the k^2-weighted EXAFS function for Pt(IV)SBA15 after heat treatment in He at (a) room temperature (as-synthesized) and (b) 250 °C (k^2: $\Delta k = 3.0 - 10.3$ Å^{-1}). The spectra are offset for clarity.

As demonstrated by TGA, the molecular precursors **1** and **2** decompose upon treatment at 250 °C, and therefore, these are poor references. In addition, the Pt centers could be partially reduced (i.e., Pt(IV) to Pt(II)). Since the exact structure of the supported Pt centers at 250 °C is unknown, the XANES spectra were fit with a linear combination of Pt foil and Pt(II)SBA15 or Pt foil and Pt(IV)SBA15. From this fit, the fraction of metallic Pt was determined to be 0.65 and 0.60, respectively. Alternatively, the fraction of metallic Pt can be estimated from the Pt−E coordination number (N_{Pt-E}). Again, since the structure of the oxidized Pt is unknown, this represents an approximation. Assuming the oxidation state of nonmetallic Pt is 2+, compounds of which often have a coordination number of 4, the estimated fraction of oxidized Pt was determined to be 0.50 (i.e., 2.0/4). The metallic fraction was also determined to be 0.50 (1 − fraction of oxidized Pt). Considering the fraction of metallic Pt determined by each method, the true metallic coordination number was estimated to be between 4 and 5, (2.5/0.6 and 2.5/0.5), respectively, which corresponds to 1 nm diameter particles.

The particle size can also be estimated from the Pt−Pt bond distance. A previous report details the determination of the coordination number, bond distance, and dispersion from hydrogen chemisorption for fully reduced Pt particles with diameters ranging from 1 to 10 nm.[76] As the particle size decreased below ∼3 nm, a contraction of the metallic bond distance was observed.[76] For fully reduced Pt, a bond distance of 2.71 Å is consistent with particles of 1 nm diameter. Particles of this size have a N_{Pt-Pt} value of about 4. Considering this bond distance method, the fraction of metallic Pt in Pt(IV)$SBA15_{250}$ was estimated to be ∼0.60 (2.5/4). This particle size is in good agreement with those estimated from a linear combination fit of the XANES data and from the N_{Pt-E} value. These analyses suggest that the initial decomposition products are very small metallic nanoparticles of ∼1 nm diameter with 6−13 atoms (i.e., N_{Pt-Pt} of 4−5). It is worth noting that Pt^0 was not detected using PXRD or TEM for PtSBA15 materials that were calcined at 250 °C under an inert atmosphere.

Oxide-supported, mononuclear Pd and Au centers have been shown to exhibit stability against cluster formation at low temperatures, but relatively mild heat treatments typically lead to agglomeration of metal centers. For example, isolated Pd atoms on MgO were stable at 27 °C for the cyclotrimerization of acetylene, but clusters were detected after heat treatment at 127 °C.[23] Mononuclear $Me_2Au(III)$ fragments on MgO were unstable after heating at 50 °C, and the Au cluster diameter increased with increasing temperature from 3 Å at 50 °C to 30 Å at 300 °C.[28] In contrast, TMP-derived Cu(I)SBA15 materials exhibited high thermal stability, with 95% of Cu sites stable as Cu(I) after treatment at 300 °C under inert atmosphere.[52] The supported mononuclear Pt sites derived from **1** and **2** are stable as isolated Pt(II) and Pt(IV) centers to relatively high temperatures (150 − 200 °C) under inert atmospheres. The decomposition temperatures are similar to those of the molecular precursors. The robust nature of the isolated Pt(II) and Pt(IV) centers can be attributed in part to the mild preparation conditions used for grafting the thermally stable molecular precursors and to the high spatial dispersity of the resulting isolated Pt sites.

Catalytic Alkene Hydrogenation. The results for the hydrogenation of styrene and cyclohexene in benzene-d_6, as catalyzed by the PtSBA15 materials under 1 atm of hydrogen, are presented in Table 4. Little substrate hydrogenation occurred after 24 h at room temperature, but more substantial conversion was observed after 24 h at 50 °C. Ethyl benzene and cyclohexane, respectively, were identified

(76) Miller, J. T.; Kropf, A. J.; Zha, Y.; Regalbuto, J. R.; Delannoy, L.; Louis, C.; Bus, E.; Van Bokhoven, J. A. *J. Catal.* **2006**, *240*, 222.

Table 4. Results of Pt-Catalyzed Styrene and Cyclohexene Hydrogenation after 24 h at 50 °C under 1 atm of H_2

	styrene		cyclohexene	
catalyst	yield (%)[a]	TON[b]	yield (%)[a]	TON[b]
Pt(II)SBA15	19	27	40	39
Pt(IV)SBA15	41	59	51	44
Pt(IV)SBA15$_{500}$			86	
1	88[c]	20	87[c]	17
2	74	11	57	8.0

[a] Yield determined by integration in the ^{1}H NMR spectrum versus an internal standard. [b] TON = mol product (mol Pt)$^{-1}$ taken at 24 h. [c] Black precipitate forms during reaction.

by ^{1}H NMR spectroscopy as the products of the reactions. In addition to the substrate hydrogenation product, the Pt(II)SBA15 catalyst liberated cyclooctane (0.60 equiv per Pt atom) after 24 h at 50 °C. In contrast, no ligand hydrogenation products were observed for the Pt(IV)SBA15 catalyst, but it is possible that gaseous CH_4 formed in an undetectable concentration. For both substrates, the Pt(IV)SBA15 catalyst demonstrated higher activity than the Pt(II)SBA15 catalyst with respect to yield and turnover number (TON, mol product (mol Pt)$^{-1}$), during 24 h. However, a catalyst with Pt nanoparticles, Pt(IV)SBA15$_{500}$, demonstrated superior activity for cyclohexene hydrogenation compared to both site-isolated catalysts.

For comparison to the supported Pt centers, the molecular precursors **1** and **2** were tested as catalysts for the hydrogenation of both substrates. In contrast to the supported catalysts, precursor **1** was approximately twice as active (vs **2**) with respect to turnover number (Table 4). However, for the reactions catalyzed by **1**, cyclooctane (1.0 equiv) and multiple siloxide resonances were observed in the ^{1}H NMR spectrum. In addition, a black precipitate rapidly formed at 50 °C, which is likely Pt^0. Thus, the hydrogenation activity exhibited by **1** was accompanied by decomposition and cannot be attributed solely to the molecular complex. For the reactions catalyzed by **2**, a small amount of HOSi(O^{t}Bu)$_3$ was detected (0.20 equiv), but no black precipitate was observed. This suggests that the Pt(IV) center is more robust toward decomposition under the reaction conditions. However, the formation of small amounts of Pt^0 from **2** under the reaction conditions cannot be excluded. The results of these reactions suggest that the supported Pt centers may also decompose under the reaction conditions to form catalytic sites (presumably Pt clusters or Pt^0) that are more efficient for hydrogenation than the as-synthesized Pt centers. It is worth noting that after catalytic testing, the Pt(II)SBA15 materials changed color from white to a pale gray. This color change was also observed for the Pt(II)- and Pt(IV)SBA15$_{500}$ materials and accompanied the formation of Pt^0 (vide supra). To investigate this, the PtSBA15 materials were examined by TEM after catalytic testing; however, within the resolution of the instrument (~2 nm), no Pt particles could be definitively resolved from the thick SBA15 framework walls.

Conclusions

The tris(*tert*-butoxy)siloxy platinum complexes **1** and **2** were synthesized in high yields and were structurally characterized via single crystal X-ray diffraction. These precursors served as excellent sources for introduction of uniform, site-isolated Pt(II) and Pt(IV) centers on the silica surface via a low-temperature protonolysis reaction with surface Si−OH groups. Due to the direct Pt−OSi linkages, **1** and **2** serve as spectroscopic models for the supported Pt sites. The supported Pt(II) and Pt(IV) centers retain many structural similarities to the molecular precursors. Similar to the precursors, little variation in the supported Pt environment was observed below the decomposition temperature of 150−200 °C. On the basis of the robust nature of the supported Pt centers, these materials offer a unique opportunity to study catalytic activity at a mononuclear, supported Pt site. The investigation of these materials as heterogeneous catalysts is of interest with respect to a number of chemical transformations (i.e., hydrogenation, hydroarylation, hydrosilation, methane oxidation). The structure sensitivity associated with some Pt catalyzed reactions has been well-documented within the limit of nanoparticles, and these TMP-derived materials hold potential to extend reactivity parameters (i.e., activation energy, selectivity, turnover frequency) to a mononuclear center.

Acknowledgment. The authors gratefully acknowledge the support of the Director, Office of Energy Research, Office of Basic Energy Sciences, Chemical Sciences Division, of the U.S. Department of Energy under Contract DE-AC03-76SF00098. We thank A. M. Stacy and A. P. Alivisatos at the University of California, Berkeley, for use of instrumentation (PXRD, SAXS, and TEM). Use of the Advanced Photon Source was supported by the U.S. Department of Energy, Office of Science, Office of Basic Energy Sciences and the MRCAT member institutions.

Supporting Information Available: X-ray crystallographic data (and CIF files) for **1** and **2**. DSC (under N_2) and TGA (under O_2) traces for **1** and **2**. SAXS patterns and TEM images of the PtSBA15 materials. FTIR spectra of **1**, **2**, and the PtSBA15 materials. This information is available free of charge via the Internet at http://pubs.acs.org.

CM801598K